

Communication

# Dual Inhibition of AChE and BChE with the C-5 Substituted Derivative of Meldrum's Acid: Synthesis, Structure Elucidation, and Molecular Docking Studies

Haroon Mehfooz <sup>1,\*</sup>, Aamer Saeed <sup>1,\*</sup>, Anamika Sharma <sup>2</sup>, Fernando Albericio <sup>2,3,4</sup>, Fayaz Ali Larik <sup>1,\*</sup>, Farukh Jabeen <sup>5</sup>, Pervaiz Ali Channar <sup>1</sup> and Ulrich Flörke <sup>6</sup>

<sup>1</sup> Department of Chemistry Quaid-i-Azam University, Islamabad 45320, Pakistan; haroonqau83@gmail.com (H.M.); mrpervaiz@gmail.com (P.A.C.)

<sup>2</sup> School of Chemistry and Physics, University of KwaZulu-Natal, Durban 4001, South Africa; anamika.aug14@gmail.com (A.S.); albericio@ukzn.ac.za (F.A.)

<sup>3</sup> Department of Organic Chemistry, University of Barcelona, 08028 Barcelona, Spain

<sup>4</sup> CIBER-BBN, Networking Centre on Bioengineering, Biomaterials and Nanomedicine, Barcelona Science Park, University of Barcelona, 08028 Barcelona, Spain

<sup>5</sup> Cardiovascular and Metabolic Research Unit, Laurentian University 935 Ramsey Lake Road, Sudbury, ON P3E 2C6, Canada; farree2005@gmail.com

<sup>6</sup> Department Chemie, Fakultät für Naturwissenschaften, Universität Paderborn, Warburgerstrasse 100, 33098 Paderborn, Germany; floerke@mail.upb.de

\* Correspondence: aamersaeed@yahoo.com (A.S.); fayazali@chem.qau.edu.pk (F.A.L.); Tel.: +92-51-9064-2128 (A.S.); Fax: +92-51-9064-2241 (A.S.)

Academic Editor: José A. Gavira

Received: 23 May 2017; Accepted: 5 July 2017; Published: 9 July 2017

**Abstract:** Alzheimer's disease (AD) lies in the category of those diseases which are still posing challenges to medicinal chemists, and the search for super-effective drugs for the treatment of AD is a work in progress. The inhibition of cholinesterase is considered a viable strategy to enhance the level of acetylcholine in the brain. The C-5 substituted derivative of Meldrum's acid was synthesized and screened against acetylcholinesterase (AChE) and butyrylcholinesterase (BChE) enzyme inhibition activity. The simple and unique structure of synthesized derivative **3** was found to be good for the dual inhibition of both enzymes (AChE and BChE). 2,2-Dimethyl-5-((2-(trifluoromethyl)phenylamino)methylidene)-1,3-dioxane-4,6-dione (**3**) showed significant inhibition against AChE, with an IC<sub>50</sub> value of 1.13 ± 0.03 μM (Standard Neostigmine 22.2 ± 3.2 μM), and moderate inhibition against BChE, with an IC<sub>50</sub> value of 2.12 ± 1.22 μM (Standard Neostigmine 49.6 ± 6.11 μM). The structural insights reveal that compound **3** possesses intriguing reactive groups, which can potentially evoke the non-covalent interactions and possibly assist by binding in the active site of the target protein. Docking simulations revealed that the compound **3** showed binding inside the active site gorges of both AChE and BChE. An excellent agreement was obtained, as the best docked poses showed important binding features mostly based on interactions due to oxygen atoms and the aromatic moieties of the compound. The docking computations coupled with the experimental findings ascertained that the compound **3** can serve as a scaffold for the dual inhibitors of the human acetylcholine esterases.

**Keywords:** Meldrum's acid derivative; synthesis; crystal study; dual inhibition; AChE and BChE; SAR; Molecular Docking; DFT

## 1. Introduction

Alzheimer's disease (AD) is a neurodegenerative disorder characterized by the loss of memory and consciousness. The rapid prevalence of AD among elderly people is expected to increase 3 times by 2050 [1]. AD poses social and economic threats to both developing and developed countries throughout the world [2]. To impede the onset and progress of AD is the ultimate challenge for medicinal chemists. Currently, a cholinergic hypothesis is the sole guideline to resolve the loss of acetylcholine, a vital neurotransmitter which helps in the communication of nerve and motor cells. A decline in the level of acetylcholine causes impairment in the cognitive functions of the human brain. Despite having moderate success rate in the cure of AD, these prescribed drugs suffer from adverse effects such as nausea and diarrhea. In addition to this, the sustainability of the drug for the prolonged treatment of AD has raised questions on these drugs. To develop effective acetylcholinesterase inhibitors (AChEI), the activity of acetylcholinesterase (AChE) must be inhibited at the oxyanion hole site (AS) and peripheral anionic site (PAS), because binding AChE at PAS results in the accumulation of amyloid- $\beta$  peptide plaques. To improve the drug to function effectively, inhibitors must bind at PAS in order to impede the function of AChE. Various classes of compounds have been reported as potent inhibitors of cholinesterase, including organophosphates, coumarin and cinnamide, acyl thioureas, acridones, chalcones, 2,3-dihydroquinazolin-4(1*H*)-one, polyamine ligands, acrylonitriles, morpholine derivatives, 2*H*-2-chromenones, and tetracyclic terpenes [3–25].

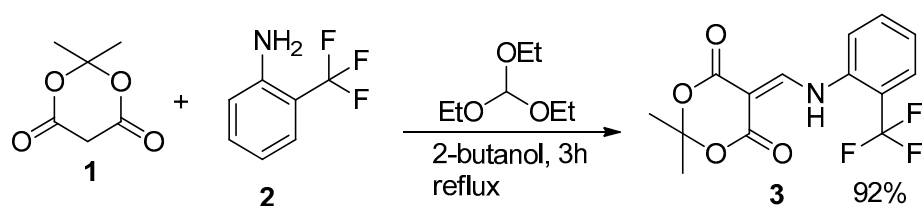
As an extension of our ongoing research on cholinesterase inhibitors (AChEI), we herein report the dual inhibitor for the acetylcholinesterase and butyrylcholinesterase enzymes. 2,2-Dimethyl-1,3-dioxane-4,6-dione, commonly known as Meldrum's acid, has been named after Andrew Norman Meldrum since 1908 [26]. Initially, the structure of Meldrum's acid (MA) was incorrectly assigned, and after several years Davidson and Bernhard elucidated the correct structure in 1948. MA is a multifaceted and versatile organic reagent, and its propensity stems from its unique but simple structure [27]. MA serves as a valuable synthon for the synthesis of nitrogen containing six-membered and other heterocyclic compounds [28]. The simplicity of its structure combined with its remarkable reactivity makes MA a reagent of choice for organic synthetic chemists. The dual nature of intrinsic chemical reactivity (electrophilic and nucleophilic) of MA paves the way for the transformation of diverse classes of organic synthetic and natural products [29]. The C (5) position of MA is enolizable, and can act as the nucleophilic centre for a wide variety of electrophilic centers, including carbonyl compounds. The C (5) position of MA provides an improved and metal-free approach to construct C-C linkages in organic molecules. The unusually high acidity (p*K*<sub>a</sub> of 4.83–4.936 in H<sub>2</sub>O) of active methylene in MA at C (5) provides direct access to the formation of a C-C framework [30]. In contrast to the C (5) position, C (4) and C (6) are susceptible to nucleophilic attack [31]. Moreover, the derivatives of MA can take active part in Knoevenagel condensation and Michael addition reactions [32].

Apart from extensive utility in organic synthesis, Meldrum's acid derivatives show biological potential as anti-malarial and antioxidant agents. Along these lines, we report a novel dual inhibitor of cholinesterase enzymes. The results of the inhibition of AChE and butyrylcholinesterase (BChE) are in the micromolar range.

## 2. Results and Discussion

### 2.1. NMR Studies

The title compound (**3**) was obtained in excellent yield by reacting Meldrum's acid (**1**) with 2-trifluoromethyl aniline (**2**) in the presence of triethyl orthoformate in 2-butanol, as shown in Scheme 1. The purity of the product was confirmed by thin layer chromatography, using ethyl acetate and *n*-hexane, ethanol, and *n*-hexane solvent systems in different compositions.



**Scheme 1.** Synthetic route towards the synthesis of a novel Meldrum's acid derivative (3).

The synthesized compound **3** was characterized by  $^1\text{H-NMR}$ ,  $^{13}\text{C-NMR}$ , DEPT  $90^\circ$ , DEPT- $135^\circ$  and EI-MS spectrometry. In  $^1\text{H-NMR}$ , the appearance of the signal at 9.5 ppm was assigned to the N-H proton. The protons attached to the  $\text{sp}^2$  carbons appeared at  $\delta$  7–8 ppm, while a singlet was observed for the methyl groups. In  $^{13}\text{C-NMR}$  spectroscopy, the appearance of a signal at around 210–200 ppm value was assigned to the carbonyl group. The methylene carbon sandwiched between two carbonyls appeared deshielded at around 80–70 ppm. The characteristic signals for aromatic carbons appeared at a value of 140–120 ppm, while carbons associated with  $\text{sp}^3$  hybridized carbon appeared at less than a value of 30–20 ppm. The EI-MS spectrum was analyzed, and the mass fragmentation pattern showed a loss of acetone and retro-Diels-Alder as the main types of fragmentation pattern.

The nature of carbon atoms was characterized through DEPT-NMR spectroscopy. In addition, the positive signals for methyl and methine confirmed the presence of these carbons.

## 2.2. X-ray Structural Study and Theoretical Calculations

The molecular structure of **3** is related to that of 5-(((2,5-Dimethylphenyl)amino)methylene)-2,2-dimethyl-1,3-dioxane-4,6-dione (QOPXEZ) [33], apart from the different phenyl-group substitution.

Two intra-molecular hydrogen bonds N1-H1 ... F3 and N1-H1 ... O1 with H1 ... F3 2.87 and H1 ... O1 2.71 Å, respectively, fix the molecular conformation to almost planarity with torsion angles C8-N1-C1-C2 177.11(17), C14-C13-C8-N1 2.6(3), and C1-C2-C3-O1 166.59(18). The geometry of the amino-methylene group shows bond lengths of C8-N1 1.416(2), N1-C1 1.330(2), and C1-C2 1.373(2) Å, and angles of C8-N1-C1 126.13(15) and N1-C1-C2 124.08(16) (Figure 1). Weaker intermolecular hydrogen bonds C1-H1A—O4 ( $-x + 1/2, -y + 1/2, -z + 1$ ) with H ... O 3.20 Å and C9-H9A ... O4 ( $-x + 1/2, -y + 1/2, -z + 1$ ) with H ... O 3.29 Å link the molecules into centrosymmetric dimers that are stacked along [010] (Figure 2).

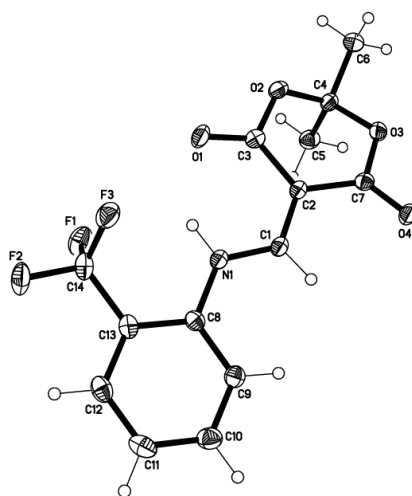


**Figure 1.** Molecular structure of **3** with anisotropic displacement ellipsoids drawn at the 50% probability level.

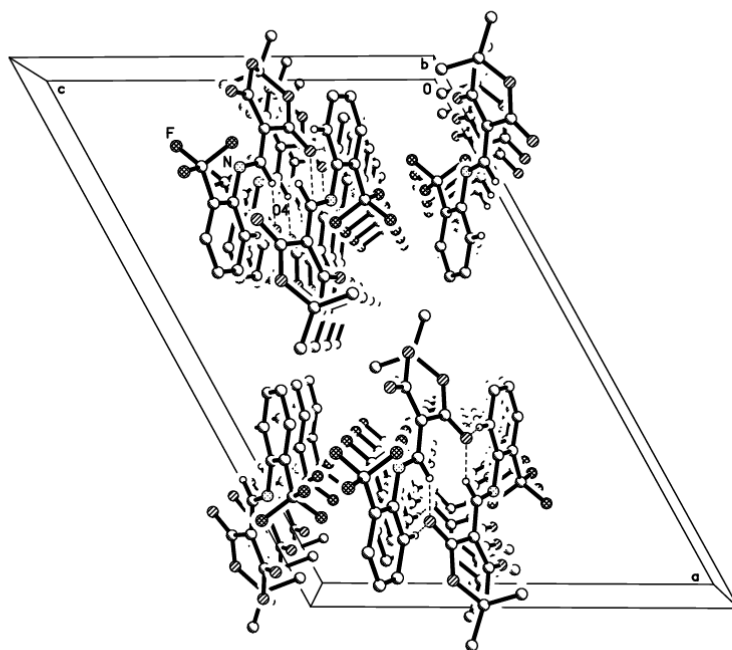


**Figure 2.** Crystal packing of **3** viewed along [010] with the H-bonding pattern as dashed lines. Hydrogen atoms not involved are omitted.

Density functional theory (DFT) geometry optimization was made on a crystal unit using the Gaussian09 program package [30], employing the Becke three parameters Lee–Yang–Parr exchange correlation functional (B3LYP) [34,35] and 6-311G++(d,p) as the basis set. The optimized geometry results in the free molecule state were compared to those in the crystalline state. No negative vibrational modes were obtained. The optimized geometry of the compound revealed a  $C2/c$  space group. The optimized geometry of the studied compounds was compared with the structural parameters obtained from the crystallographic information file (CIF). All of the bond lengths and angles calculated were in agreement with the crystal structure. The optimized structure is as shown in Figure 3. No puckering was observed in the aromatic six-membered ring between atoms C(24)–C(25)–C(27)–CO(29)–C(31)–C(33). However, puckering was observed between C(12)–C(13)–O(5)–C(14)–O(6)–C(23). Bifurcated intramolecular H-bonding interactions can be seen between N(8)–H(9) and F(3) as well as between N(8)–H(9) and O(4) with an interatomic distance of 2.8 Å and 1.9 Å, respectively, which is well in agreement with the crystal structure.

The Total Energy and Frontier Orbital energy levels were also calculated using DFT. The geometry of the title compound was optimized using DFT method in the gas phase. The crystal structure of **3** was used for the DFT studies. The energy gap between the HOMO and the LUMO was calculated by the B3LYP method using 6-311G++(d,p) as the basis set. The title compound shows energy gap ( $\Delta E = 0.16506$  Hartree = 4.45 eV) for HOMO  $\rightarrow$  LUMO (Figure 3). The HOMO and LUMO are important factors that affect bioactivity, chemical reactivity, electron affinity, and ionization potential [36]. Thus, the study of the frontier orbital energy can provide useful information about the biological reaction mechanism as discussed in the docking section later.

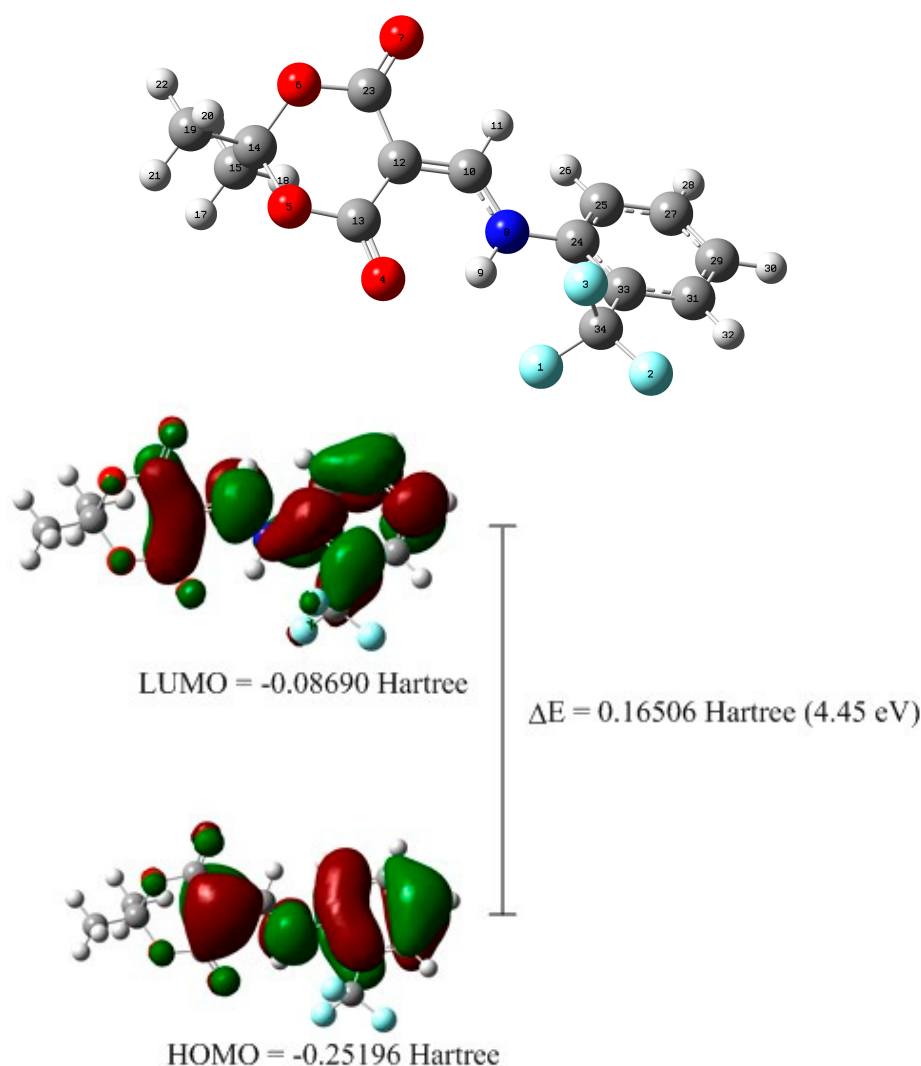


**Figure 3.** Optimized geometry and frontier molecular orbitals of the compound **3**.

### 2.3. Acetylcholinesterase and Butyrylcholinesterase Inhibition Assay

The synthesized compound **3** was screened against Acetylcholinesterase (AChE) and butyrylcholinesterase (BChE) enzyme inhibition activities. The synthesized compound **3** showed inhibition in the micromolar range. Interestingly, compound **3** was found to be a dual inhibitor of both enzymes (AChE and BChE). The  $IC_{50}$  value of compound **3** was found to be  $1.13 \pm 0.03 \mu M$ , and this result is several times better than the standard Neostigmine ( $22.2 \pm 3.2 \mu M$ ). The BChE inhibition results were also found to be of moderate significance, and the derivative **3** exhibited inhibition with an  $IC_{50}$  value of  $2.12 \pm 1.22 \mu M$  compared to the reference Neostigmine ( $49.6 \pm 6.11 \mu M$ ) (Table 1). The induction of trifluoromethyl moiety further results in the enhancement of enzyme inhibition activity. The presence of fluorine atoms in the bioactive molecules paves the way for effective drug designing, because fluorine atoms, being the most electronegative, can show or induce polar interactions. The presence of the N-H group can act as a hydrogen bonding receptor. The results of inhibition against AChE and BChE represent higher potency at the micromolar level when compared to Neostigmine. However, compound **3** shows less potency when compared to donepezil and tacrin, because both these commercial drugs show inhibition at the nanomolar level. Compound **3** exhibits better potential compared to Rivastigmine and Galantamine. Overall, compound **3** shows moderate activity at the micromolar level.

**Table 1.** Dual AChE and BChE inhibition activity.

Compound	AChE Activity	BChE Activity
	IC <sub>50</sub> (μM) ± SEM	
3	1.13 ± 0.03	2.12 ± 1.22
Neostigmine	22.2 ± 3.2	49.6 ± 6.11
Donepezil	6.4 ± 0.4 nM	33.65 nM
Tacrine	45.1 ± 7 nM	3.2 ± 0.2 nM
Rivastigmine	501 ± 3.08 μM	19.95 ± 0.20 μM
Galantamine	4 ± 0.13 μM	7.96 ± 0.59 μM

SEM means standard error of mean.

#### 2.4. Docking Computation

To further understand the binding interaction of these proteins, we used computational docking of the compounds to Acetylcholine esterases. In particular, compound **3** was found to interact favorably with the AChE and BChE proteins, with a docking and Glide score of  $-7.04$  and  $-6.55$  kcal/mol, respectively. The active site for both of the targets was found to be a deep narrow cavity, and compound **3** bound itself inside the active site of both the targets.

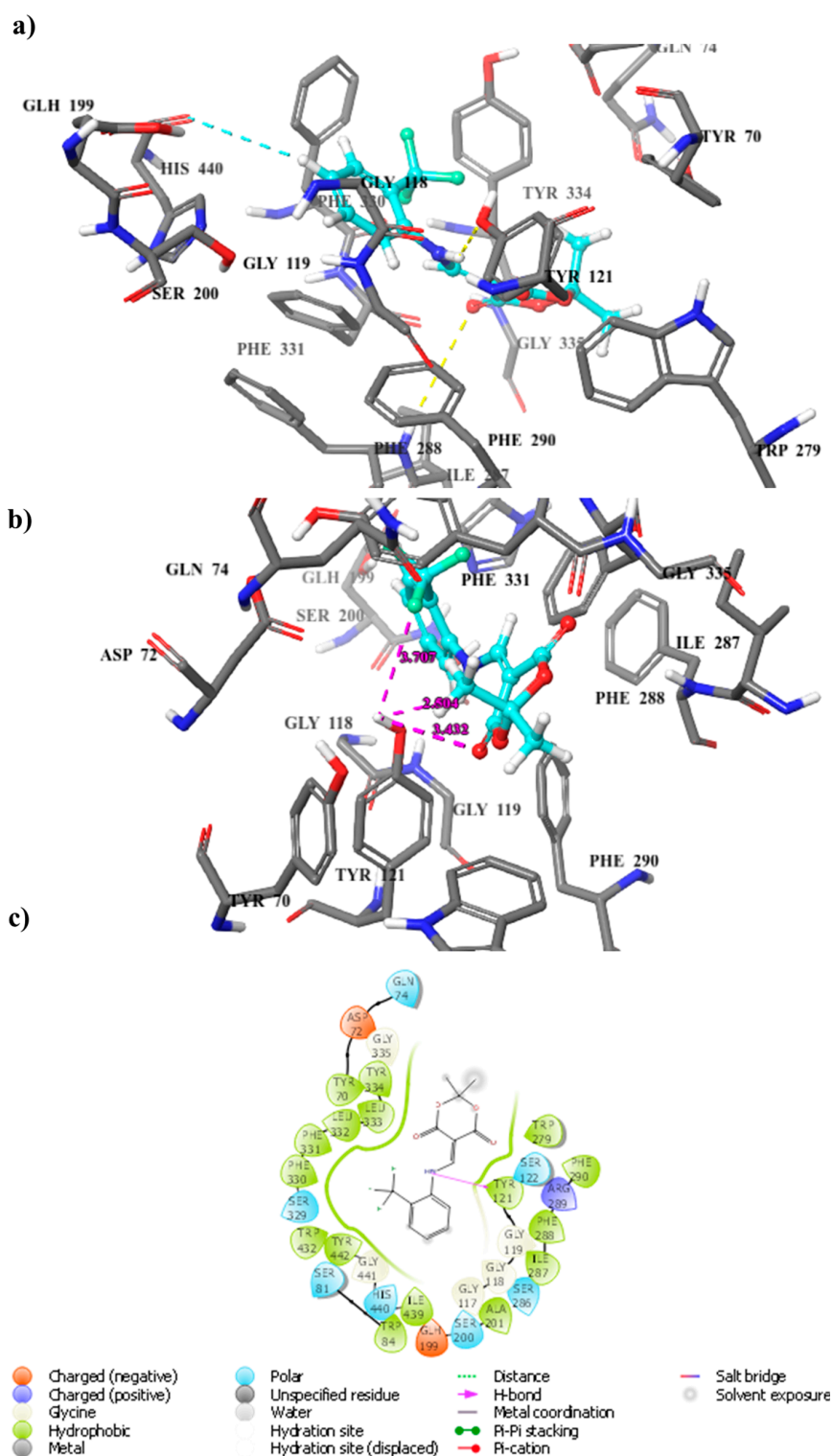
Based on the initial assessment of the binding pose for the AChE docking, we found that residues such as Gly118, Try121, Phe288, Tyr334, and His 440 are key residues. The lactone part of the compound **3** established robust hydrogen bonding with Gly118, providing an anchoring point for the flanking regions to interact with the protein (Figure 4a). It is also interesting to note that the compound occupied the binding site, forming a halogen-bonding with Gly118 through the terminal fluorine group as shown in Figure 4b. The hydrogen of the phenyl ring established aromatic hydrogen bonding with His440, which provided another anchoring point to the compound **3** inside the active site gorge of AChE (Figure 4a). Figure 4c represents the orientation of the compound **3** inside the active site gorge of AChE in two dimensional space.

A Detailed analysis of the binding mode of the best docked conformation of the compound **3** revealed that Trp82, Ser198, Gly117, Ala199 and His438, Phe329, Val288, Trp231, Ser287, Gly110, Ala199, Trp82, and His438 are key interacting residues; the interaction of compound **3** with these can influence the catalytic function of the enzyme.

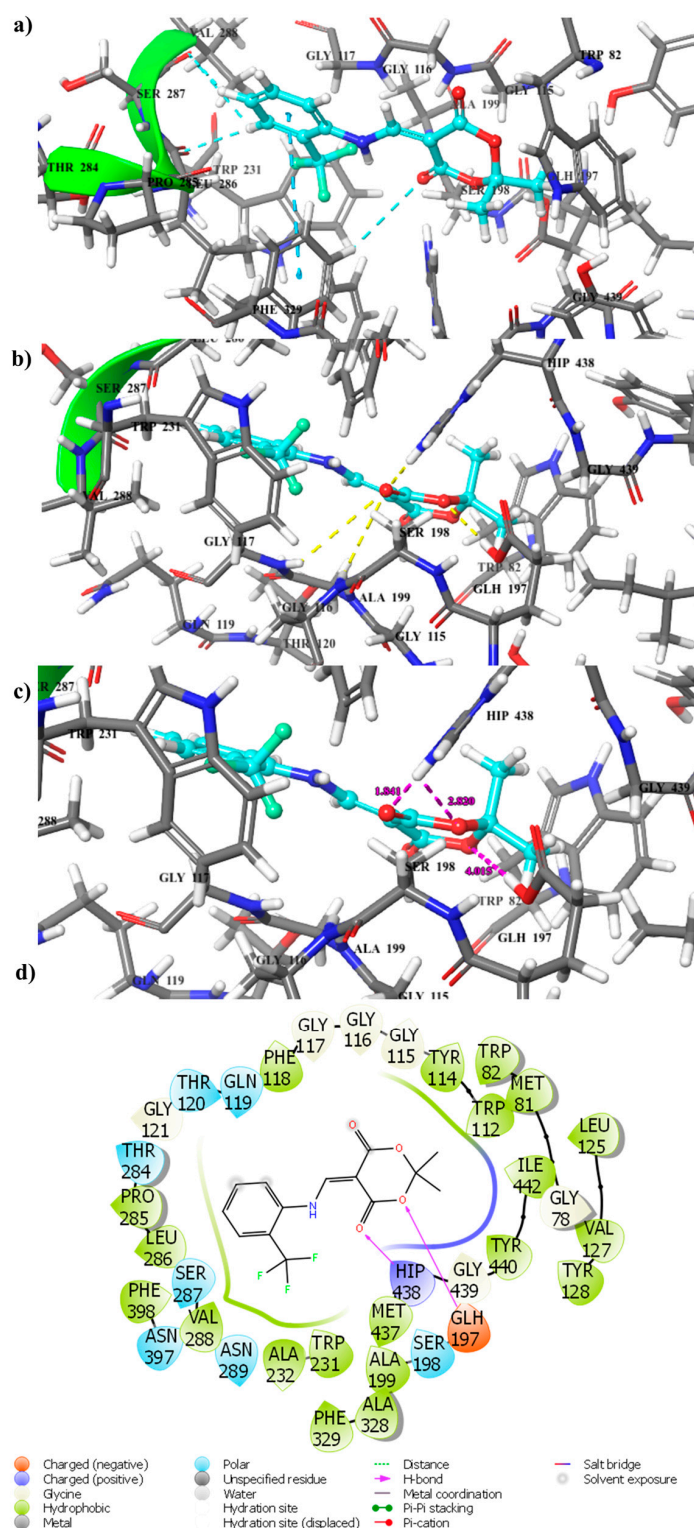
The compound **3** anchored itself inside the active site gorge by establishing strong  $\pi$ - $\pi$  interactions, hydrogen bonding, and aromatic hydrogen bonding with key residues such as Phe329, Val288, Trp231, Ser287, Gly110, Ala199, Trp82, and His438. Trp82 was present inside the primary binding site, and Trp238 was present at the peripheral part of the binding pocket; both interacted with the compound through hydrogen bonding and aromatic hydrogen bonding, respectively (Figure 5a–d). Hydrogen of the terminal phenyl group formed aromatic hydrogen bonding inside the active site in addition to strong  $\pi$ - $\pi$  stacking with Phe329, which stabilized the binding of the terminal phenyl group; however, the other end of the compound showed differential binding interaction. Compound **3** also established determinant contacts with the key residues through strong hydrogen bonding. The acid portion of the compound played a significant role in the binding of molecules by developing couios strong hydrogen bonding with key residues such as Trp82, Ser198, Gly117, Ala199, and His438.

Figure 5a–c represents the docking pose of ligand **3** inside the active site of BChE in tri-dimensional space, and Figure 5d shows the docking pose of ligand **3** inside the active site of BChE in di-dimensional space.

In *in silico* studies, compound **3** showed significant interactions and a good binding score with both the targets, which render it useful to serve the purpose of the discovery of a dual inhibitor.



**Figure 4.** Binding mode of compound 3 inside the active site of AChE. (a,b) Docking poses of compound 3 in tri-dimensional space. Ligands are shown in ball and stick mode in elemental and cyan color, and the key residues are shown by stick mode, elemental color, and green color respectively. (a) Aromatic hydrogen bonding and hydrogen and halogen bonding of ligand atoms with residue atoms is shown in pink colored dashed lines. (b) Hydrogen and halogen bonding of ligand atoms with residue atoms is shown in pink colored dashed line (c) Docking pose of compound 3 inside the active site in two dimensional space.



**Figure 5.** Binding mode of compound 3 inside the active site of BChE. (a–c) Docking poses of compound 3 in tri-dimensional space. Ligands are shown in ball and stick mode in elemental and cyan color, and the key residues are shown by stick mode, elemental color, and green color, respectively. (a) Aromatic hydrogen bonding and  $\pi$ - $\pi$  interaction of ligand atoms with residue atoms is shown in pink colored dashed lines. (b) Hydrogen bonding of ligand atoms with residue atoms is shown in pink colored dashed line (c) Hydrogen and halogen bonding of ligand atoms with residue atoms is shown in pink colored dashed line (d) Docking pose of compound 3 inside the active site in two dimensional space.

### 2.5. Drug-Like Profiling

The structure of the compound **3** was drawn, and its energy minimized, after tri-dimensional (3D) cleaning. Tri-dimensional cleaning involves the addition of hydrogen, the minimization, and the optimization of the geometry. The lowest energy conformer produced by the software was used for further calculations. The optimized geometry as shown in Figure 5 was used for the calculation of the descriptors. Several descriptors, such as rotatable bond number, hydrogen bond donor number, hydrogen bond acceptor number,  $\log P$ , molecular weight, and total polar surface area (TPSA) were computed to access the drug-like properties of the synthesized compound. The computation's results revealed that compound **3** was found to act in accordance with Lipinski's Ro5 and Veber's Ro3 cut-off limits [37], revealing the fact that these could be potent surrogates for neurodegenerative diseases.

According to Lipinski's Ro5, most drug-like molecules should have molecular weight  $\leq 500$ , logarithm of the octanol/water partition coefficient ( $\log P$ )  $\leq 5$ , total polar surface area (TPSA)  $< 140 \text{ \AA}$ , number of hydrogen bond donors (HBD)  $\leq 5$ , and number of hydrogen bond acceptors (HBA)  $\leq 10$ . Further modifications in the Ro5 were made by Veber et al. [38], who suggested that the number of rotatable bonds (NOR) of drug-like molecules must be fewer or equal to 10 [39]. Molecules violating more than one of these criteria could have problems with bioavailability. Compound **3** conforms to all of the criteria of being a drug-like molecule. The computed value of the  $\log P$  for the molecule **3** is 6.7, while all other parameters happened to fall under the prescribed criteria for a compound to be drug-like. The numeric values of all of the computed descriptors are tabulated in Table 2.

**Table 2.** Descriptors computed for compound **3**.

Entry	Descriptors Name	Computed Values
3	Number of rotatable bonds	3.00
	Hydrogen Bond Acceptor	2.0
	Hydrogen Bond Donor	0.0
	Log P (o/w) = logarithm of the (octanol/water) partition coefficient	6.7
	Total polar surface area (TPSA)	32.67
	Molecular weight	315.05

### 3. Materials and Methods

The melting point was taken three times using a Gallen Kamp apparatus. The proton magnetic resonance spectra were recorded in DMSO- $d_6$  with an Advance AV 300 spectrometer and an Advance AV 500 spectrometer operating at 300 MHz and 500 MHz, respectively. The carbon magnetic resonance spectra were recorded in DMSO- $d_6$  with an Advance AV 300 spectrometer and an Advance AV 500 spectrometer operating at 300 MHz and 500 MHz, respectively. The mass spectrum was recorded with JEOL MS route operated with Electron Ionization mode.

#### 3.1. Synthesis of 2,2-Dimethyl-5-((2-(trifluoromethyl)phenyl)Amino)methylidene)-1,3-dioxane-4,6-dione (**3**)

To a stirred solution of an equimolar quantity of Meldrum's acid (**1**) (1.0 mmol) and 2-trifluoromethyl aniline (**2**) in 2-butanol in a round bottom flask was added dropwise triethyl orthoformate (3.0 mmol). The reaction mixture was refluxed for 3 hours. The solid formed in hot state was collected by suction filtration. Washing with ethanol furnished TLC Kiesel 60 F254 from Merck pure compound in an 85% yield. The synthesized compound was recrystallized from ethanol.

Yield: 73%, dark yellow, m.p. 120 °C.  $^1\text{H}$  NMR (300MHz, DMSO- $d_6$ )  $\delta$ : 11.6 (1H, d,  $J$  12.8, CH-NH), 8.7 (1H, d,  $J$  12.8, CH-NH), 7.9 (1H, d,  $J$  8, ArH), 7.4 (1H, m,  $J$  7.7, ArH), 7.7 (1H, m, ArH), 1.7 (6H, s, 2CH<sub>3</sub>);  $^{13}\text{C}$  NMR (300MHz, DMSO- $d_6$ )  $\delta$ : 164.3 (C), 162.0 (C), 154.8 (CH), 135.8 (C) 134.4 (CH), 126.7(CH), 126.6 (CH), 126.6 (C), 120.8 (CH), 118.6 (C), 104.1 (C), 88.5 (C), 26.4 (CH<sub>3</sub>); MS (EI):  $m/z$  314.7 (M+ 7.7%), 256.7 (65.6), 211.9 (48.8), 191.9 (22.6), 113.8 (10.9), 82.9 (100), 53 (37.3). Anal Calc: C<sub>14</sub>H<sub>12</sub>F<sub>3</sub>NO<sub>4</sub>; C, 53.34, H, 3.85, N, 4.65, Found, C, 54.37, H, 4.53, N, 5.04.

### 3.2. Structure Determination

Data were collected on a Bruker APEX-II D8 Venture area diffractometer, equipped with graphite monochromatic Mo  $K\alpha$  radiation,  $\lambda = 0.71073 \text{ \AA}$  at 100 (2) K. The cell refinement and data reduction were carried out by Bruker SAINT SHELXS [37,39], which was used to solve the structure.

Crystal Structure Determination of 3: ( $C_{14}H_{12}F_3NO_4$ ),  $M_r = 315.3$ , yellow crystal, size  $0.40 \times 0.21 \times 0.16 \text{ mm}^3$ , monoclinic space group  $C 2/c$  with  $Z = 8$ ,  $a = 23.769(4)$ ,  $b = 8.1063(13)$ ,  $c = 16.127(3) \text{ \AA}$ ,  $\beta = 118.853(3)$ ,  $V = 2721.6(8) \text{ \AA}^3$ ;  $D_c = 1.539 \text{ Mg/m}^3$ ,  $\mu = 0.139 \text{ mm}^{-1}$ ,  $F(000) = 1296$ . The intensity data were recorded using a Bruker SMART CCD area-detector diffractometer with graphite monochromated Mo $K\alpha$  radiation ( $\lambda = 0.71073 \text{ \AA}$ ) at  $T = 130(2) \text{ K}$ . The number of reflections collected was 12,546:  $1.95 > \Theta > 27.88$ ; 3244 independent reflections  $I > 2\sigma(I)$ ,  $R_{\text{int}} = 0.049$ . Structure solution by direct methods<sup>X2</sup>, full-matrix least squares refinement<sup>X2</sup> based on  $F^2$  and 205 parameters. All but H-atoms were refined anisotropically; the hydrogen atoms were clearly located from difference Fourier maps, and then refined at idealized positions riding on the carbon atoms with isotropic displacement parameters  $U_{\text{iso}}(\text{H}) = 1.2U_{\text{eq}}(\text{C/N})$  or  $1.5U_{\text{eq}}(\text{CH}_3)$ , and C-H 0.95–0.99  $\text{ \AA}$ , H(N) was refined freely. Refinement converged at  $R1 = 0.045 [I > 2\sigma(I)]$ ,  $wR2 = 0.107$  (all data) and  $S = 1.02$ ; min./max.  $\Delta F = 0.22/0.34 \text{ e/\AA}^3$ .

The crystallographic data (excluding structure factors) for the structure reported in this paper have been deposited with the Cambridge Crystallographic Data Centre as supplementary publication no. CCDC-1544670. Copies of available material can be obtained free of charge via [www.ccdc.cam.ac.uk](http://www.ccdc.cam.ac.uk).

### 3.3. DFT Calculations

The starting geometries were taken from X-ray refined data. The density functional theory (DFT) geometry optimization with the Gaussian09 program package [38] using the Becke three parameters Lee–Yang–Parr (B3LYP) exchange correlation functional, which combines the hybrid exchange functional of Becke [40] with the gradient-correlation functional of Lee, Yang, and Parr [41] and the 6–311G++(d,p) basis set, was performed in a gas phase. No solvent corrections were made with these calculations, as it was reported that gas phase calculations frequently correspond well with crystal structures [42].

### 3.4. Acetylcholinesterase and Butyrylcholinesterase Inhibition Assay

The AChE and BChE inhibitory studies of synthesized derivatives were measured by using the reported Ellman's method with slight modifications [43]. Briefly, the total reaction volume was kept as 100  $\mu\text{L}$ , containing 60  $\mu\text{L}$  of phosphate buffer (50 mM  $\text{KH}_2\text{PO}_4$  pH 7.7), 10  $\mu\text{L}$  of test compound (800  $\mu\text{M}$  per well), followed by the addition of 10  $\mu\text{L}$  of AChE (0.015 unit per well) or 10  $\mu\text{L}$  of BChE (0.1 unit per well). The contents of the well were mixed homogeneously and incubated at 37  $^\circ\text{C}$  for 10 min, and the optical density was measured at 405 nm using 96 well plate reader (Bio-TekELx 800TM, Instruments, Inc.). The reaction was initiated by the addition of 10  $\mu\text{L}$  of Acetyl thiocholine chloride or butyrylthiocholine chloride as substrate (0.5 mM per well), followed by the addition of 10  $\mu\text{L}$  of coloring reagent 5, 5'-dithiobis-2-nitro benzoic acid (DTNB). The reaction mixture was incubated at 37  $^\circ\text{C}$  for 20 min, and the optical density was measured at 405 nm. Neostigmine was used as a positive control. For the compounds which exhibited over 50% inhibition of either AChE or BChE activity, full concentration, inhibition curves were produced to evaluate the  $\text{IC}_{50}$  values. All of the experiments were carried out as triplicate. A non-linear regression analysis of the program PRISM 5.0 (GraphPad, San Diego, California, CA, USA) was used to fit the dose–response curves and to calculate the  $\text{IC}_{50}$  values.

### 3.5. Molecular Docking Studies

The crystal structure of the AChE and BChE proteins was obtained from RCSB Research Collaboratory for Structural Bioinformatics (PDB (protein data bank) entry 1ACL and 1POI) [44,45],

and were utilized for modeling purposes. The crystal structures were solved in complex after cleaning, thereby providing a suitable starting point for computational studies. The proteins were prepared by adding missing hydrogens, followed by minimization and optimization using the ProteinPrep module of the Schrodinger program [46]. A grid was generated for docking purposes by creating a box centroid at the cognate ligands of each of both the AChE and BChE. The ligand **3** was prepared using the ligprep module of the Schrodinger program. The glide standard precision (Glide-SP) module was used for the docking simulations [47].

Chemaxon software [48] was used for the calculation of descriptors to access the drug-likeness profile of the compound. The structure of the compound **3** was drawn and energy minimized after 3D cleaning using chemaxon software and maestro by Schrodinger. The optimized geometry as shown in Figure 5 was used for the calculation of the descriptors.

#### 4. Conclusions

The C-5 substituted Meldrum's acid derivative **3** was synthesized and was thoroughly characterized by spectroscopic techniques including <sup>1</sup>H-NMR, <sup>13</sup>C-NMR (DEPT-135 and DEPT 90), and single crystal XRD. The crystal system is monoclinic, the space group is C 2/c, and the unit cell dimensions are a = 23.769(4) Å, α = 90°, b = 8.1063(13) Å, β = 118.853(3), c = 16.127(3) Å, γ = 90°. The title compound shows energy gap (ΔE = 0.16506 Hartree = 4.45 eV) for HOMO → LUMO.

The synthesized compound **3** was screened against acetylcholinesterase and butyrylcholinesterase enzyme inhibition activities. The results of the bioassay revealed that compound **3** possess moderate potential to act as a dual inhibitor against these two enzymes involved in neurodegenerative diseases. Docking simulations were useful in understanding the interaction of the compound **3** with both the AChE and BChE proteins. A moderate inhibitive potential exhibited by the compound **3** proclaimed it a surrogate for future investigation as a potential dual inhibitor of AChE and BChE.

**Acknowledgments:** This work was funded in part by the following: the National Research Foundation (NRF) and the University of KwaZulu-Natal (South Africa); and the CICYT (CTQ2015-67870-P), and the Generalitat de Catalunya (2014 SGR 137) (Spain).

**Author Contributions:** Haroon Mehfooz, and Aamer Saeed conceived and designed the experiments; Anamika Sharma, and Fernando Albericio performed DFT calculations and improved the manuscript significantly. X.X. performed the experiments; Farukh Jabeen and Pervaiz Ali Channar analyzed the data; Ulrich Flörke contributed reagents/materials/analysis tools; Fayaz Ali Larik wrote the paper.

**Conflicts of Interest:** Authors declare no conflict of interest.

#### References

1. Small, D.H.; San Mok, S.; Bornstein, J.C. Alzheimer's disease and aβ toxicity: From top to bottom. *Nat. Rev. Neurosci.* **2001**, *2*, 595–598. [[CrossRef](#)] [[PubMed](#)]
2. Kuruva, C.S.; Reddy, P.H. Amyloid beta modulators and neuroprotection in alzheimer's disease: A critical appraisal. *Drug Discov. Today* **2017**, *22*, 223–233. [[CrossRef](#)] [[PubMed](#)]
3. Saeed, A.; Zaib, S.; Ashraf, S.; Iftikhar, J.; Muddassar, M.; Zhang, K.Y.; Iqbal, J. Synthesis, cholinesterase inhibition and molecular modelling studies of coumarin linked thiourea derivatives. *Bioorg. Chem.* **2015**, *63*, 58–63. [[CrossRef](#)] [[PubMed](#)]
4. Saeed, A.; Mahesar, P.A.; Zaib, S.; Khan, M.S.; Matin, A.; Shahid, M.; Iqbal, J. Synthesis, cytotoxicity and molecular modelling studies of new phenylcinnamide derivatives as potent inhibitors of cholinesterases. *Eur. J. Med. Chem.* **2014**, *78*, 43–53. [[CrossRef](#)] [[PubMed](#)]
5. Mohammadi-Khanaposhtani, M.; Saeedi, M.; Zafarghandi, N.S.; Mahdavi, M.; Sabourian, R.; Razkenari, E.K.; Alinezhad, H.; Khanavi, M.; Foroumadi, A.; Shafiee, A. Potent acetylcholinesterase inhibitors: Design, synthesis, biological evaluation, and docking study of acridone linked to 1, 2, 3 triazole derivatives. *Eur. J. Med. Chem.* **2015**, *92*, 799–806. [[CrossRef](#)] [[PubMed](#)]
6. Larik, F.A.; Saeed, A.; Channar, P.A.; Ismail, H.; Dilshad, E.; Mirza, B. New 1-octanoyl-3-aryl thiourea derivatives: Solvent-free synthesis, characterization and multi-target biological activities. *Bangladesh J. Pharmacol.* **2016**, *11*, 894–902. [[CrossRef](#)]

7. Raza, A.; Saeed, A.; Ibrar, A.; Muddassar, M.; Khan, A.A.; Iqbal, J. Pharmacological evaluation and docking studies of 3-thiadiazolyl-and thioxo-1, 2, 4-triazolylcoumarin derivatives as cholinesterase inhibitors. *ISRN Pharmacol.* **2012**, *2012*, 11. [[CrossRef](#)] [[PubMed](#)]
8. Tran, T.D.; Nguyen, T.C.V.; Nguyen, N.S.; Nguyen, D.M.; Nguyen, T.T.H.; Le, M.T.; Thai, K.M. Synthesis of novel chalcones as acetylcholinesterase inhibitors. *Appl. Sci.* **2016**, *6*, 198. [[CrossRef](#)]
9. Saeed, A.; Shah, M.S.; Larik, F.A.; Khan, S.U.; Channar, P.A.; Flörke, U.; Iqbal, J. Synthesis, computational studies and biological evaluation of new 1-acetyl-3-aryl thiourea derivatives as potent cholinesterase inhibitors. *Med. Chem. Res.* **2017**, *8*, 1635–1646. [[CrossRef](#)]
10. Sultana, N.; Sarfraz, M.; Tahir, S.; SafwanAkram, M.; Sadiq, A.; Rashid, U.; Tariq, M.I. Synthesis, crystal structure determination, biological screening and docking studies of n 1-substituted derivatives of 2, 3-dihydroquinazolin-4 (1h)-one as inhibitors of cholinesterases. *Bioorg. Chem.* **2017**, *72*, 256–267. [[CrossRef](#)] [[PubMed](#)]
11. Bolognesi, M.L.; Andrisano, V.; Bartolini, M.; Banzi, R.; Melchiorre, C. Propidium-based polyamine ligands as potent inhibitors of acetylcholinesterase and acetylcholinesterase-induced amyloid- $\beta$  aggregation. *J. Med. Chem.* **2005**, *48*, 24–27. [[CrossRef](#)] [[PubMed](#)]
12. Cheung, J.; Rudolph, M.J.; Burshteyn, F.; Cassidy, M.S.; Gary, E.N.; Love, J.; Franklin, M.C.; Height, J.J. Structures of human acetylcholinesterase in complex with pharmacologically important ligands. *J. Med. Chem.* **2012**, *55*, 10282–10286. [[CrossRef](#)] [[PubMed](#)]
13. Colovic, M.B.; Krstic, D.Z.; Lazarevic-Pasti, T.D.; Bondzic, A.M.; Vasic, V.M. Acetylcholinesterase inhibitors: Pharmacology and toxicology. *Curr. Neuropharmacol.* **2013**, *11*, 315–335. [[CrossRef](#)] [[PubMed](#)]
14. Darvesh, S.; Darvesh, K.V.; McDonald, R.S.; Mataija, D.; Walsh, R.; Mothana, S.; Lockridge, O.; Martin, E. Carbamates with differential mechanism of inhibition toward acetylcholinesterase and butyrylcholinesterase. *J. Med. Chem.* **2008**, *51*, 4200–4212. [[CrossRef](#)] [[PubMed](#)]
15. Mohammadi-Khanaposhtani, M.; Mahdavi, M.; Saeedi, M.; Sabourian, R.; Safavi, M.; Khanavi, M.; Foroumadi, A.; Shafiee, A.; Akbarzadeh, T. Design, synthesis, biological evaluation, and docking study of acetylcholinesterase inhibitors: New acridone-1, 2, 4-oxadiazole-1, 2, 3-triazole hybrids. *Chem. Biol. Drug Des.* **2015**, *86*, 1425–1432. [[CrossRef](#)] [[PubMed](#)]
16. Torre, P.D.L.; Saavedra, L.A.; Caballero, J.; Quiroga, J.; Alzate-Morales, J.H.; Cabrera, M.G.; Trilleras, J. A novel class of selective acetylcholinesterase inhibitors: Synthesis and evaluation of (e)-2-(benzo [d] thiazol-2-yl)-3-heteroarylacrylonitriles. *Molecules* **2012**, *17*, 12072–12085. [[CrossRef](#)] [[PubMed](#)]
17. Sukumaran, S.D.; Chee, C.F.; Viswanathan, G.; Buckle, M.J.; Othman, R.; Abd Rahman, N.; Chung, L.Y. Synthesis, biological evaluation and molecular modelling of 2'-hydroxychalcones as acetylcholinesterase inhibitors. *Molecules* **2016**, *21*, 955. [[CrossRef](#)] [[PubMed](#)]
18. Munoz-Ruiz, P.; Rubio, L.; García-Palomero, E.; Dorransoro, I.; Del Monte-Millán, M.; Valenzuela, R.; Usán, P.; De Austria, C.; Bartolini, M.; Andrisano, V. Design, synthesis, and biological evaluation of dual binding site acetylcholinesterase inhibitors: New disease-modifying agents for alzheimer's disease. *J. Med. Chem.* **2005**, *48*, 7223–7233. [[CrossRef](#)] [[PubMed](#)]
19. Parveen, M.; Aslam, A.; Nami, S.A.; Malla, A.M.; Alam, M.; Lee, D.U.; Rehman, S.; Silva, P.P.; Silva, M.R. Potent acetylcholinesterase inhibitors: Synthesis, biological assay and docking study of nitro acridone derivatives. *J. Photochem. Photobiol. B Biol.* **2016**, *161*, 304–311. [[CrossRef](#)] [[PubMed](#)]
20. Piazzzi, L.; Rampa, A.; Bisi, A.; Gobbi, S.; Belluti, F.; Cavalli, A.; Bartolini, M.; Andrisano, V.; Valenti, P.; Recanatini, M. 3-(4-([benzyl (methyl) amino] methyl) phenyl)-6, 7-dimethoxy-2 h-2-chromenone (ap2238) inhibits both acetylcholinesterase and acetylcholinesterase-induced  $\beta$ -amyloid aggregation: A dual function lead for alzheimer's disease therapy. *J. Med. Chem.* **2003**, *46*, 2279–2282. [[CrossRef](#)] [[PubMed](#)]
21. Raza, R.; Saeed, A.; Arif, M.; Mahmood, S.; Muddassar, M.; Raza, A.; Iqbal, J. Synthesis and biological evaluation of 3-thiazolocoumarinyl schiff-base derivatives as cholinesterase inhibitors. *Chem. Biol. Drug Des.* **2012**, *80*, 605–615. [[CrossRef](#)] [[PubMed](#)]
22. Sauvâtre, T.; Barlier, M.; Herlem, D.; Gresh, N.; Chiaroni, A.; Guenard, D.; Guillou, C. New potent acetylcholinesterase inhibitors in the tetracyclic triterpene series. *J. Med. Chem.* **2007**, *50*, 5311–5323. [[CrossRef](#)] [[PubMed](#)]
23. Tasso, B.; Catto, M.; Nicolotti, O.; Novelli, F.; Tonelli, M.; Giangreco, I.; Pisani, L.; Sparatore, A.; Boido, V.; Carotti, A.; et al. Quinolizidiny derivatives of bi-and tricyclic systems as potent inhibitors of acetyl- and

- butyrylcholinesterase with potential in Alzheimer's disease. *Eur. J. Med. Chem.* **2011**, *46*, 2170–2184. [[CrossRef](#)] [[PubMed](#)]
24. Bartorelli, L.; Giraldi, C.; Saccardo, M.; Cammarata, S.; Bottini, G.; Fasanaro, A.M.; Trequattrini, A. Effects of switching from an AChE inhibitor to a dual AChE-BuChE inhibitor in patients with Alzheimer's disease. *Curr. Med. Res. Opin.* **2005**, *21*, 1809–1817. [[CrossRef](#)] [[PubMed](#)]
  25. Nicolotti, O.; Pisani, L.; Catto, M.; Leonetti, F.; Giangreco, I.; Stefanachi, A.; Carotti, A. Discovery of a Potent and Selective Hetero-Bivalent AChE Inhibitor via Bioisosteric Replacement. *Mol. Inform.* **2011**, *30*, 133–136. [[CrossRef](#)] [[PubMed](#)]
  26. Li, J.S.; Da, Y.D.; Chen, G.Q.; Yang, Q.; Li, Z.W.; Yang, F.; Huang, P.M. Solvent-, and catalyst-free acylation of anilines with meldrum's acids: A neat access to anilides. *ChemistrySelect* **2017**, *2*, 1770–1773. [[CrossRef](#)]
  27. Çalışkan, R.; Nohut, N.; Yılmaz, Ö.; Sahin, E.; Balci, M. Unusual manganese (iii)-mediated oxidative free-radical additions of meldrum's acid and dimethyl malonate to benzonorborene and oxabenzonorborene. *Tetrahedron* **2017**, *73*, 291–297. [[CrossRef](#)]
  28. Gopakumar, D.A.; Pasquini, D.; Henrique, M.A.; De Morais, L.C.; Grohens, Y.; Thomas, S. Meldrum's acid modified cellulose nanofiber-based polyvinylidene fluoride microfiltration membrane for dye water treatment and nanoparticle removal. *ACS Sustain. Chem. Eng.* **2017**, *5*, 2026–2033. [[CrossRef](#)]
  29. Zhang, J.W.; Xue, J.H.; Zhang, H.H.; Xu, F.; Chen, Q.G.; Li, J.H. Reaction of meldrum's acid with an aminomethylating agent and nitroalkanes. *J. Chem. Res.* **2017**, *41*, 72–74. [[CrossRef](#)]
  30. Ivanov, A.S. Meldrum's acid and related compounds in the synthesis of natural products and analogs. *Chem. Soc. Rev.* **2008**, *37*, 789–811. [[CrossRef](#)] [[PubMed](#)]
  31. De Toledo, T.; Da Silva, L.; Teixeira, A.; Freire, P.; Pizani, P. Characterization of meldrum's acid derivative 5-(5-ethyl-1, 3, 4-thiadiazol-2-ylamino) methylene-2, 2-dimethyl-1, 3-dioxane-4, 6-dione by raman and ft-ir spectroscopy and dft calculations. *J. Mol. Struct.* **2015**, *1091*, 37–42. [[CrossRef](#)]
  32. Sandhu, H.S.; Sapra, S.; Gupta, M.; Nepali, K.; Gautam, R.; Yadav, S.; Kumar, R.; Jachak, S.M.; Chugh, M.; Gupta, M.K. Synthesis and biological evaluation of arylidene analogues of meldrum's acid as a new class of antimalarial and antioxidant agents. *Bioorg. Med. Chem.* **2010**, *18*, 5626–5633. [[CrossRef](#)] [[PubMed](#)]
  33. Rotzoll, S.; Reinke, H.; Fischer, C.; Langer, P. Synthesis of novel halogenated 4 (1H)-quinolones by thermolysis of arylaminomethylene-1, 3-dioxane-4, 6-diones. *Synthesis* **2009**, *1*, 69–78. [[CrossRef](#)]
  34. Frisch, M.J.; Trucks, G.W.; Schlegel, H.B.; Scuseria, G.E.; Robb, M.A.; Cheeseman, J.R.; Scalmani, G.; Barone, V.; Mennucci, B.; Petersson, G.A.; et al. *Gaussian 09*; Gaussian, Inc.: Wallingford, CT, USA, 2009.
  35. Becke, A.D. Density-functional exchange-energy approximation with correct asymptotic behavior. *Phys. Rev. A* **1988**, *38*, 3098. [[CrossRef](#)]
  36. Lee, C.; Yang, W.; Parr, R.G. Development of the colle-salvetti correlation-energy formula into a functional of the electron density. *Phys. Rev. B* **1988**, *37*, 785. [[CrossRef](#)]
  37. Jabeen, F.; Oliferenko, P.V.; Oliferenko, A.A.; Pillai, G.G.; Ansari, F.L.; Hall, C.D.; Katritzky, A.R. Dual inhibition of the  $\alpha$ -glucosidase and butyrylcholinesterase studied by molecular field topology analysis. *Eur. J. Med. Chem.* **2014**, *80*, 228–242. [[CrossRef](#)] [[PubMed](#)]
  38. Lipinski, C.A.; Lombardo, F.; Dominy, B.W.; Feeney, P.J. Experimental and computational approaches to estimate solubility and permeability in drug discovery and development settings. *Adv. Drug Del. Rev.* **1997**, *23*, 3–25. [[CrossRef](#)]
  39. Veber, D.F.; Johnson, S.R.; Cheng, H.Y.; Smith, B.R.; Ward, K.W.; Kopple, K.D. Molecular properties that influence the oral bioavailability of drug candidates. *J. Med. Chem.* **2002**, *45*, 2615–2623. [[CrossRef](#)] [[PubMed](#)]
  40. Sheldrick, G. *Shelxtl-pc (Version 5.1)*; Siemens Analytical Instruments, Inc.: Madison, WI, USA, 1997.
  41. Sheldrick, G.M. A short history of shelx. *Acta Crystallogr. Sect. A Found. Crystallogr.* **2008**, *64*, 112–122. [[CrossRef](#)] [[PubMed](#)]
  42. Neese, F.; Wennmohs, F.; Hansen, A.; Becker, U. Efficient approximate and parallel Hartree-Fock and hybrid DFT calculations. A 'chain-of-spheres' algorithm for the Hartree-Fock exchange. *Chem. Phys.* **2009**, *356*, 98–109. [[CrossRef](#)]
  43. Honarparvar, B.; Govender, T.; Maguire, G.E.; Soliman, M.E.; Kruger, H.G. Integrated approach to structure-based enzymatic drug design: Molecular modeling, spectroscopy, and experimental bioactivity. *Chem. Rev.* **2013**, *114*, 493–537. [[CrossRef](#)] [[PubMed](#)]
  44. Ellman, G.L.; Courtney, K.D.; Andres, V.; Featherstone, R.M. A new and rapid colorimetric determination of acetylcholinesterase activity. *Biochem. Pharmacol.* **1961**, *7*, 88–90. [[CrossRef](#)]

45. Harel, M.; Schalk, I.; Ehret-Sabatier, L.; Bouet, F.; Goeldner, M.; Hirth, C.; Axelsen, P.; Silman, I.; Sussman, J. Quaternary ligand binding to aromatic residues in the active-site gorge of acetylcholinesterase. *Proc. Natl. Acad. Sci. USA* **1993**, *90*, 9031–9035. [[CrossRef](#)] [[PubMed](#)]
46. Nicolet, Y.; Lockridge, O.; Masson, P.; Fontecilla-Camps, J.C.; Nachon, F. Crystal structure of human butyrylcholinesterase and of its complexes with substrate and products. *J. Biol. Chem.* **2003**, *278*, 41141–41147. [[CrossRef](#)] [[PubMed](#)]
47. Schrödinger, L. *Schrödinger Suite 2016-4 Protein Preparation Wizard*, Epik, version; Schrödinger, Inc.: New York, NY, USA, 2016; Volume 2.
48. ChemAxon. Marvin. Marvinn.n.n (versionnumber), 201n. Available online: <http://www.chemaxon.com> (accessed on 9 July 2010).



© 2017 by the authors. Licensee MDPI, Basel, Switzerland. This article is an open access article distributed under the terms and conditions of the Creative Commons Attribution (CC BY) license (<http://creativecommons.org/licenses/by/4.0/>).